AIMS Energy, 6(6): 1032–1049.
DOI: 10.3934/energy.2018.6.1032
Received: 15 October 2018
Accepted: 13 December 2018
Published: 17 December 2018

http://www.aimspress.com/journal/energy

Research article

Development of walkway blocks with high water permeability using waste glass fiber-reinforced plastic

Yusuke Yasuda[1], Hayato Iwasaki[2], Kentaro Yasui[3], Ayako Tanaka[2] and Hiroyuki Kinoshita[3,*]

[1] Interdisciplinary Graduate School of Agriculture and Engineering, University of Miyazaki, 1-1 Gakuen-Kibanadai-Nishi, Miyazaki 889-2192, Japan
[2] Graduate School of Engineering, University of Miyazaki, 1-1 Gakuen-Kibanadai-Nishi, Miyazaki 889-2192, Japan
[3] Faculty of Engineering, University of Miyazaki, 1-1 Gakuen-Kibanadai-Nishi, Miyazaki 889-2192, Japan

* **Correspondence:** Email: t0d165u@cc.miyazaki-u.ac.jp; Tel: +81985587290; Fax: +81985582876.

Abstract: To utilize waste glass fiber-reinforced plastic (GFRP), we have created porous ceramics by mixing crushed GFRP with clay and then firing the resultant mixture. Some GFRP/clay ceramics have great porosity, which allows water to pass through them. In this study, by exploiting the high strength and water permeability of GFRP/clay ceramics, we aimed to develop water-permeable paving blocks that could prevent the inundation of roads by sudden heavy rains in urban areas. Various specimens were made by adjusting the mixing ratio of clay and crushed GFRP (40–60 mass%), the GFRP particle size, and the firing temperature. Bending strength, compressive strength, and permeability tests were then carried out on the samples. The obtained values were compared with those of porous ceramics made by mixing plastic without glass fiber and clay before firing. First, the difference in the porosity and strength of GFRP/clay ceramics and porous ceramics without glass fiber was clarified. Then, the manufacturing conditions of ceramics that satisfy both strength and permeability criteria were clarified for water-permeable paving blocks.

Keywords: waste GFRP; recycling; ceramic; paving block; water permeability; strength

1. Introduction

Glass fiber-reinforced plastic (GFRP) is used in various products, such as automobile parts. However, most waste GFRP is presently sent to a landfill. Fine glass fiber dust and leachates from disposal sites may cause serious health problems and environmental damage, and landfill sites may also become unavailable in the future because of space constraints [1–4]. To conserve resources and reduce the environmental burden, it is important to develop an effective technique for the disposal of waste GFRPs without polluting the environment.

In general, development of new products from waste cannot succeed without making the manufacturing cost low and demonstrating a clear advantage for the waste as a raw material [5]. Considering this, attempts to create functional materials by using waste plastics have been conducted, mainly in the field of concrete materials. These methods are expected to grow in the future as a means to effectively use discarded GFRP. However, since many GFRPs are currently landfilled, it is desirable to develop further effective utilization methods of waste GFRP [6–13].

We have therefore proposed a process that produces GFPR ceramics by mixing crushed waste GFRP with clay and then firing the resultant mixture (termed GFRP/clay ceramics) [14–16]. This process is not sensitive to the type of GFRP, and it can also minimize fine glass fiber dust generation due to sintering between the clay and glass fiber or between glass fibers. In the ceramic manufacturing process, a clay-based ceramic with a high porosity can be produced because the resin components in GFRP thermally decompose during firing process, and the ceramic clay matrix is reinforced with glass fibers [14–16]. Some ceramics allow water to pass through [17]. Therefore, we have focused on the sudden localized heavy rains that are occurring more frequently due to global warming. More specifically, we have targeted the development of water-permeable paving blocks [18–20] to prevent the inundation of urban roads caused by sudden heavy rain.

Various type of GFRPs are currently produced. These GFRPs contain up to approximately 60 mass% glass fiber, mostly E glass. In considering the application of GFRP/clay ceramics to water-permeable pavement blocks, first, it is very important to know the porosity and strength of the ceramics and then to clarify the difference of GFRP ceramics from those of porous ceramics without glass fiber.

In this study, various specimens were made by adjusting the mixing ratio of clay and crushed GFRP, the particle size of GFRP, and the firing temperature using three types of GFRPs, which contained glass fibers of approximately 40, 50, and 60 mass%. The porosity, strength, and permeability of the ceramic specimens were measured. The porosity and strength of the GFRP/clay ceramics were investigated in detail by comparison with those of porous ceramics, which were made by mixing clay and resin without glass fiber. Then, the manufacturing conditions that satisfy both the strength and permeability criteria required for water-permeable paving blocks were investigated.

2. Materials and methods

2.1. Production of GFRP/clay ceramics

Figure 1 shows the manufacturing process for GFRP/clay ceramics. Three types of plastic pellets containing glass fiber at approximately 40%, 50%, and 60% by mass were used as waste GFRPs. For 40%GF/GFRP and 60%GF/GFRP, which contained glass fiber of 40 and 60 mass%,

respectively, polyamide (PA) thermoplastic pellets (Renny, Mitsubishi Engineering-Plastics Co., Japan) were used, and for 50%GF/GFRP, phenol thermoset plastic pellets (PM-9640, Sumitomo Bakelite Co., Ltd., Japan) were used.

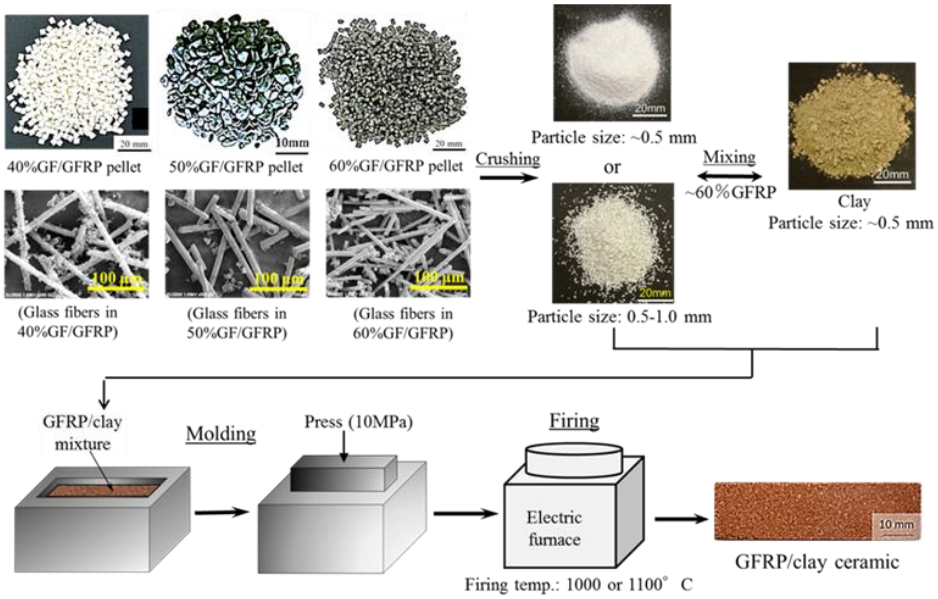

Figure 1. Manufacturing process of GFRP/clay ceramic.

The glass fibers shown in Figure 1 are SEM images of the residues after heating GFRP pellets at 400 ℃. From the SEM images, it is estimated that 40%GF/GFRP contained glass fibers with diameters of approximately 10 μm and lengths of ~1.0 mm, and 50%GF/GFRP contained glass fibers with diameters of approximately 10 μm and lengths of ~1.5 mm. The size of the glass fibers included in 60%GF/GFRP was approximately 7 μm in diameter and ~0.5 mm long. Thus, the glass fibers included in 60%GF/GFRP were slightly thinner and shorter than those of the other GFRPs.

Clay produced in Miyazaki, Japan, for the manufacture of brick or tile was used. Table 1 shows the inorganic chemical compositions of the GFRPs and clay after firing at 800 ℃. The major mineral in the clay was from the chlorite group. Here, clay is classified broadly into two types [21]. One is a porcelain basis material containing kaolinite as the major mineral. The other is an earthenware basis material containing chlorite as the major mineral. The porcelain basis material after firing possesses little water-absorption ability, but the earthenware basis material does have porosity. We selected clay containing chlorite with a high water-absorption ability to produce paving blocks with a high water permeability. Ceramics with high water-absorption capacity may also have a heat island mitigation effect as a water-retentive paving block [22].

Table 1. Chemical compositions of inorganic substances in clay and GFRP.

Component	Clay (chlorite) (mass%)	40%GF/GFRP (mass%)	50%GF/GFRP (mass%)	60%GF/GFRP (mass%)
SiO_2	65.8	36.1	51.3	51.5
Al_2O_3	21.9	10.1	14.2	14.8
Fe_2O_3	4.79	0.37	0.28	0.37
K_2O	3.37	0.12	0.16	0.16
MgO	1.67	1.53	2.76	2.52
CaO	1.31	50.9	30.1	29.9
TiO_2	0.87	0.59	0.35	0.33

We made rectangular specimens that had a length of 70 mm, width of 20 mm, and thickness of approximately 5–10 mm for bending strength tests; cylindrical specimens with a diameter of 14 mm and length of approximately 35 mm for compressive tests; and disc-shaped specimens with a diameter of ~44 mm and thickness of 10 mm for permeability tests as follows:

(1) Clay was crushed using a rotary mill (New Power Mill PM-2005, Osaka Chemical Co., Ltd., Japan) and then sifted using a 0.5 mm mesh screen.
(2) GFRP was also crushed using the rotary mill, and then sifted using a 0.5 or 1.0-mm mesh screen.
(3) 0–60% crushed GFRP by total mass was mixed with the clay.
(4) The mixture was solidified by pressing it into a mold at 10 MPa.
(5) The molded samples were heated in an oxidizing atmosphere at 100 ℃ h^{-1} to the firing temperature (1,000 or 1,100 ℃) using an electric furnace (KY-4N, Kyoei Electric Kilns Co., Ltd., Japan). Samples were held at the firing temperature for 1 h and then cooled to room temperature in the furnace.

Figure 2a shows the particle size distribution of the clay after sifting. Figure 2b shows microscope images of 50%GF/GFRP powder sifted using a 0.5 or 1.0-mm mesh screen. The maximum length of the GFRP powder was approximately 1.0 mm when using a 0.5-mm mesh screen, and approximately 2.0 mm when using a 1.0-mm mesh screen. The size distributions of the other GFRP powders after sifting were almost the same.

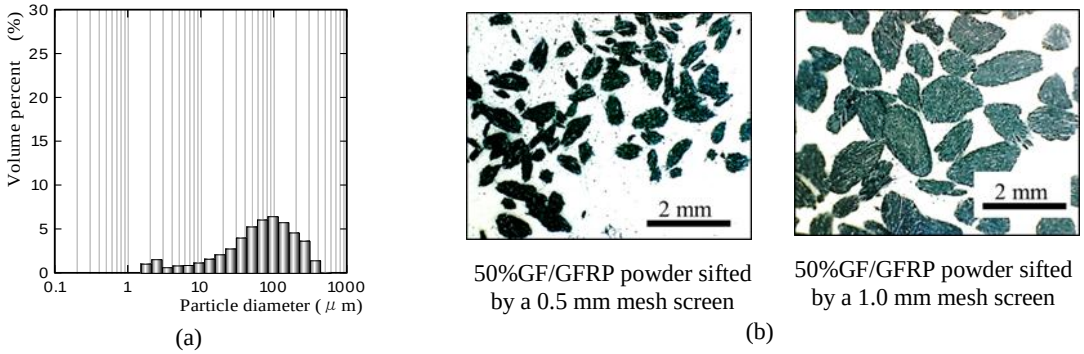

(a) (b)

Figure 2. (a) Particle size distribution of clay; (b) microscope images of 50%GF/GFRP powder sifted using a 0.5- or 1.0-mm mesh screen.

2.2. Experimental methods

2.2.1. Measurement of ceramic apparent porosity

To investigate the relationship between the porosity and strength or permeability on GFRP/clay ceramics, the apparent porosity was measured on the basis of Japanese Industrial Standard (JIS) R2205:1992. In addition, the apparent porosities and pore-diameter distributions of many ceramics were measured using a mercury porosimeter (Auto Pore IV 9500, Micromeritics Instrument Corp., USA).

2.2.2. Strength test of ceramics

To determine the manufacturing conditions under which GFRP/clay ceramics satisfy the bending and compressive strength criteria [23] required for water-permeable paving blocks, four-point bending and uniaxial compression tests were carried out. The tests were performed using a universal testing machine (AG-X50kN, Shimadzu Corp., Japan) with a crosshead speed of 0.5 mm min^{-1}. Maximum bending stress was calculated from the measured maximum load. Compressive strength was obtained by dividing the measured maximum compressive load by the specimen cross-sectional area.

2.2.3. Water permeability test of ceramics

Ceramic permeability tests were carried out on the basis of the falling-head permeability test of soil in JIS A1218:2009. Figure 3 shows a schematic illustration of the permeability test. The ceramic permeability was evaluated by calculating the coefficient of permeability:

$$k_{\mathrm{T}} = 2.303 \frac{aL}{A(t_2 - t_1)} \log_{10} \frac{h_1}{h_2} \tag{1}$$

where k_{T} is the coefficient of permeability, a is the cross-sectional cylinder area, L is the specimen thickness, A is the cross-sectional specimen area, and h_1 and h_2 are the water levels at times t_1 and t_2, respectively. In Figure 3, the internal cylinder diameter was 46 mm and the cylinder cross-sectional area a was 1,662 mm^2. The specimen thickness L was 10 mm, and the net cross-sectional area A, excluding the area of the specimen covered with a sealing material, was 841 mm^2.

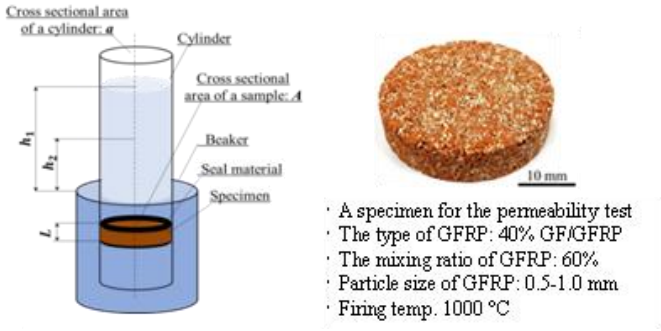

Figure 3. Schematic illustration of permeability test.

3. Results and discussions

3.1. Apparent porosity of GFRP/clay ceramics

Figures 4a, b shows the appearance of GFRP/clay ceramic specimens made by mixing 40%GFRP with clay and examples of the ceramic surface structure, respectively. Particulate matter is the glass fibers remaining in the clay structure after firing. It can be seen that the glass fibers in the clay structure were sintered and formed larger agglomerates.

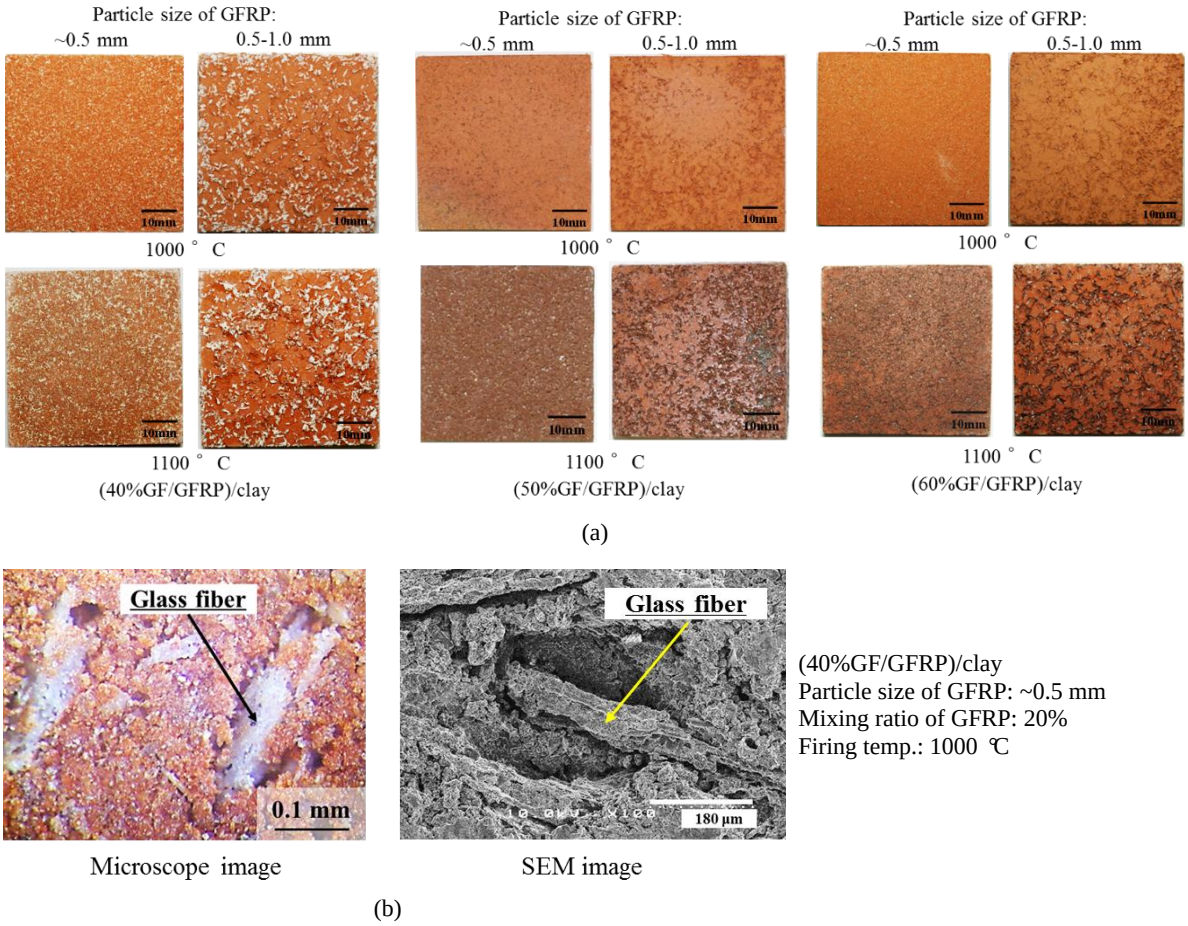

Figure 4. (a) Examples of GFRP/clay ceramics; and (b) ceramic surface structure.

Figure 5 shows the apparent porosities of GFRP/clay ceramics. The porosities of ceramics fired at 1,000 ℃ increased with increasing GFRP mixing ratio. This is because the amount of resin also increases with increasing mixing ratio, and the resin component decomposes during firing, which creates voids in the ceramic structure.

The apparent porosities of the ceramics fired at 1,100 ℃ did not necessarily increase with increasing GFRP mixing ratio. Particularly, the apparent porosities of ceramics made under the conditions that the GFRP particle size was ~0.5 mm and the GFRP mixing ratio was 60% could not be measured because the ceramic structure almost melted during the firing process. However, the ceramic structure did not melt when using the GFRP with a particle size of 0.5–1.0 mm. This

means that the ceramic made using the GFRP with a particle size of ~0.5 mm was easier to melt than that made using the GFRP with a particle size of 0.5–1.0 mm. The reasons for this are considered to be as follows.

The softening and melting points of the glass fibers included in GFRPs were in temperature ranges of 700–1,000 ℃ and less than 1,200 ℃ [24,25], respectively. The melting point of clay was approximately 1,200 ℃ [14,21]. Thus, the melting point of the glass fiber was a little lower than that of clay. When using the GFRP with a particle size of ~0.5 mm, the GFRP/clay sample molded before firing contained GFRP particles more evenly inside the body than when using GFRP with the particle size of 0.5–1.0 mm because the number of GFRP particles was larger. Therefore, when using the GFRP with a particle size of ~0.5 mm, more atoms are thought to be diffused between glass fibers during the firing process, so that the ceramic structure almost transformed to a molten state.

The results in Figure 5 show that ceramics with porosities of approximately 20–60% or higher were produced when they were fired at 1,000 ℃, and those with the porosity of 50% or higher were produced when they were fired at 1,100 ℃. In addition, a ceramic with a significantly low porosity was also produced due to melting of the glass fiber.

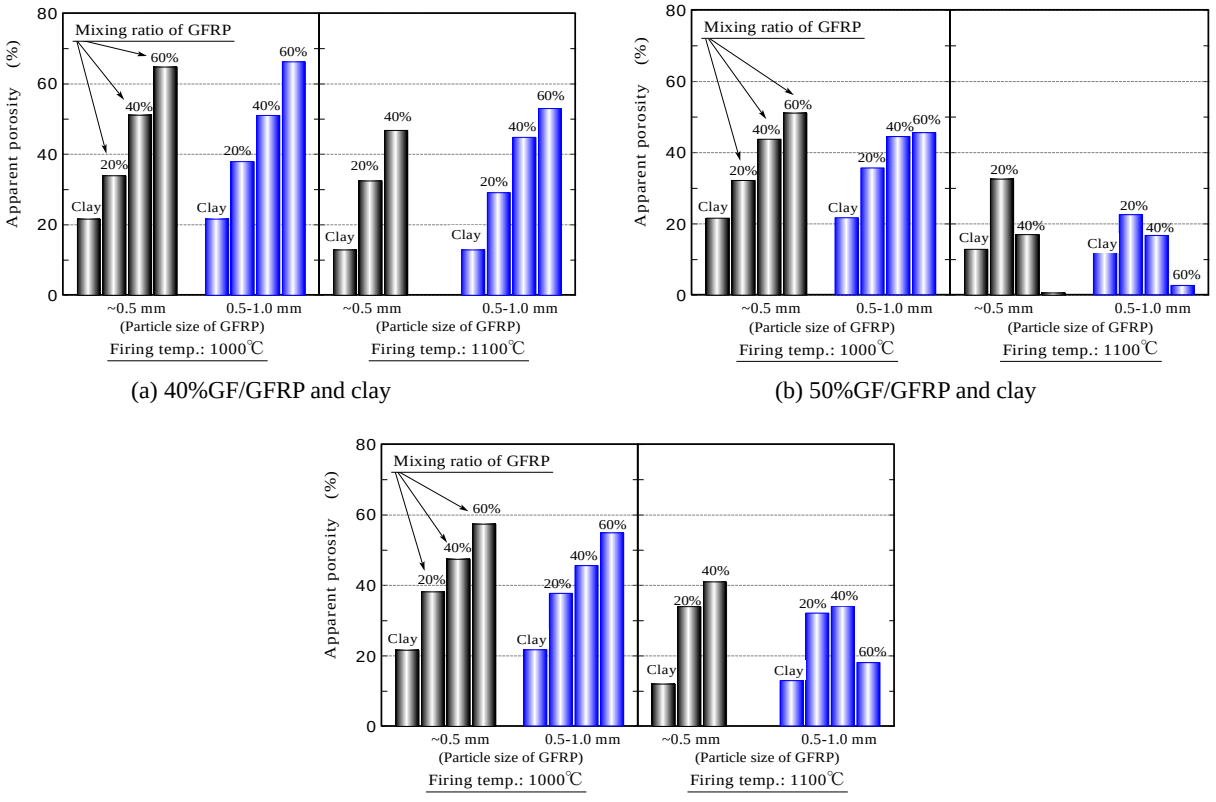

(a) 40%GF/GFRP and clay

(b) 50%GF/GFRP and clay

(c) 60%GF/GFRP and clay

Figure 5. Apparent porosities of GFRP/clay ceramics.

Figure 6 shows the porosity versus resin mixing ratio of GFRP/clay ceramics. In the diagrams, the porosities of PA resin/clay ceramics, which were made from clay and PA resin without glass fiber, are plotted along with those of GFRP/clay ceramics. Here, when 40%GF/GFRP was mixed with clay at a mixing ratio of 10%, the mixing ratio of the resin corresponds to 6%. When fired at 1,000 ℃, the

porosities of GFRP/clay ceramics increased nearly linearly with increase in the resin mixing ratio regardless of GFRP particle size. When fired at 1,100 ℃, the ceramic porosities were not proportional to the resin mixing ratio. Particularly, the porosity of the 50%GF/GFRP and clay ceramic decreased with increasing resin mixing ratio at GFRP mixing ratios of 20% or more.

To investigate the reason for the decreased porosity, we measured the linear thermal expansions of glass fibers included in the GFRPs by performing thermomechanical analysis (TMA) (TMA4200SA, Bruker AXS, Germany). The measurement was carried out in keeping with JIS R2207-3:2007. Here, the glass fibers used for the TMA were prepared by heating a GFRP pellet at 400 ℃ and then molding it into a square rod at 30 MPa. The rod was 15 × 15 mm square and 15 mm long. Then, the longitudinal dimensional change of the specimen while being heated at 5 ℃ min^{-1} was measured.

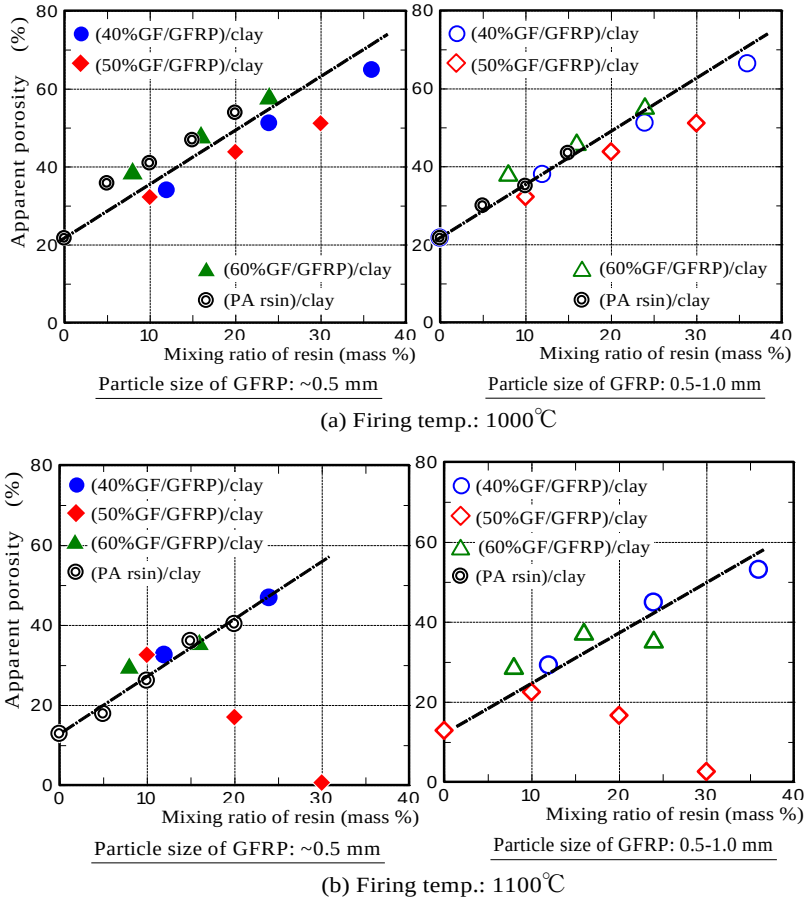

Figure 6. Relationship between apparent ceramic porosity and resin mixing ratio.

Figure 7 shows the relationships between temperature or time and linear thermal expansion on glass fibers included in the three GFRPs. In the graphs, negative linear thermal expansion means that the specimen shrank. It was found that the glass fiber in 50%GF/GFRP began to shrink at around 700 ℃, and the fiber in 40%GF/GFRP began to shrink at around 740 ℃. The specimen shrinkage is considered to have resulted from sintering between glass fibers. Therefore, the reason why the porosity of 50%GF/GFRP and clay ceramic fired at 1,100 ℃ decreased with increasing resin mixing ratio is thought to be that the sintering process between glass fibers increased markedly.

Here, the softening point of a glass fiber is defined as the temperature at which it elongates at a rate of 1 mm min^{-1} by its own weight. From the slope at the end of the graph shown in Figure 7b, the glass fiber is presumed to have been included in 50%GF/GFRP possessed the lowest softening point, and that included in 40%GF/GFRP possessed the highest softening point.

On the basis of the above results, the porosities of GFRP/clay ceramics fired at 1,100 ℃ are thought to depend on the mixing ratio and the particle size of GFRP. Practically, GFRP includes various kinds of filling materials in addition to glass fiber [26]. Therefore, the softening point of the inorganic matter included in GFRP may differ considerably from that of glass fiber. Therefore, it remains difficult to predict accurately the relationship between GFRP mixing ratio and the porosity of the produced ceramic. It is necessary to research the relationship ratio by ratio.

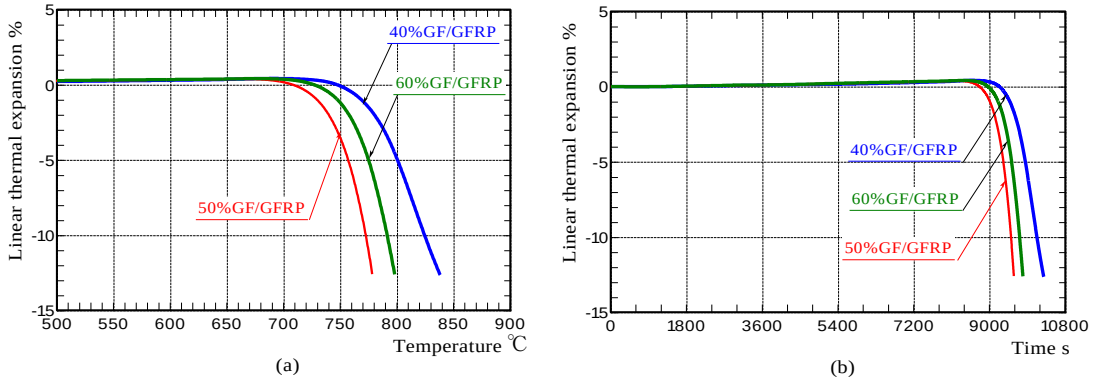

Figure 7. Relationship between temperature and linear thermal expansion on glass fibers included in 40%GF/GFRP and 60%GF/GFRP by TMA.

3.2. Ceramic bending strength

In general, ceramics have a disadvantage in that the variation in their strength can be large. Thus, caution is required to use them as structural materials. The fracture of a GFRP/clay ceramic may also depend on multiple factors, such as its porosity and the strength of the glass fibers. Therefore, we analyzed the Weibull distribution of the bending strength of GFRP/clay ceramics.

Figure 8 shows Weibull plots of the bending strength of GFRP/clay and PA resin/clay ceramics. The *x*- and *y*-axes express logarithms of bending strength and specimen cumulative failure probability *P*, respectively. For the 60%GF/GFRP and clay ceramics, the bending strengths of ceramics made using GFRP with particle sizes of 1.0–1.4 mm are also shown. The bending strengths were examined additionally on the basis of the results of compressive strength and permeability tests of the ceramics, which are discussed below.

Weibull plots of the bending strength of GFRP/clay ceramics could be generally approximated by a straight line. The bending strength decreased with increase in mixing ratio of GFRP except for some of the ceramics with 50%GF/GFRP and also decreased with increasing GFRP particle size. This is because ceramic porosity increased when the GFRP mixing ratio increased, and the voids generated in the ceramic structure caused stress concentrations.

Comparing the bending strength of each GFRP/clay ceramic, the bending strength of ceramics with 50%GF/GFRP was relatively higher than those of the other GFRP/clay ceramics. The glass

fibers and clay matrix were presumed to have been sintered more strongly than those of other ceramics because the glass fiber in 50%GF/GFRP had the lowest shrinkage start temperature.

A bending strength of 3 MPa or greater is required for water-permeable blocks [23]. Table 2 shows the manufacturing conditions of GFRP/clay ceramics that satisfy the bending strength criterion. Some ceramics fired at 1,000 ℃ and most of the ceramics fired at 1,100 ℃ met this criterion.

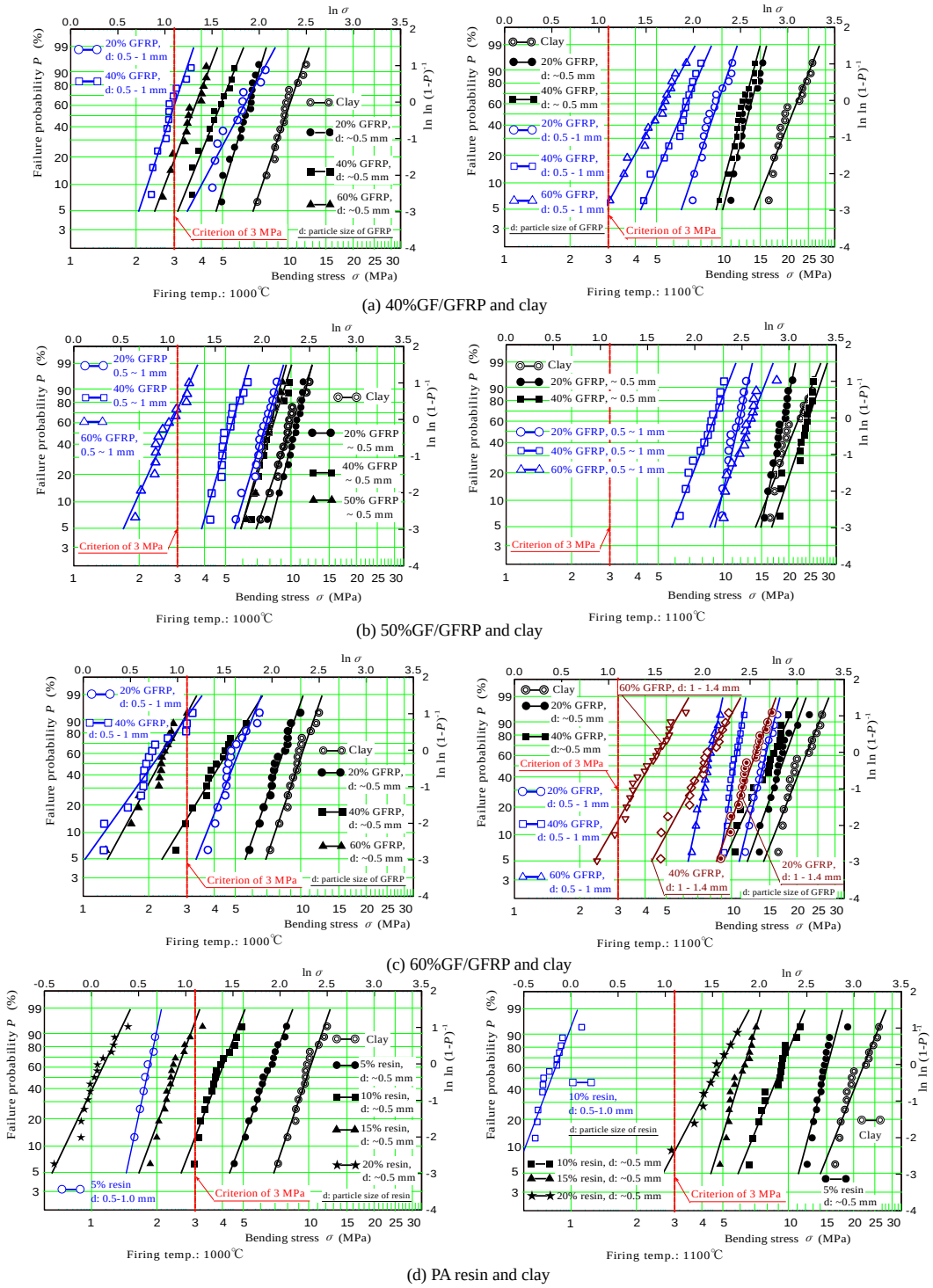

(a) 40%GF/GFRP and clay

(b) 50%GF/GFRP and clay

(c) 60%GF/GFRP and clay

(d) PA resin and clay

Figure 8. Bending strength of ceramics made with GFRP and PA resin.

Table 2. GFRP/clay ceramic manufacturing conditions that satisfy the bending strength criterion of 3 MPa or greater.

Ceramic type	GFRP mixing ratio (mass%)	GFRP particle size (mm)	Firing temp (℃)
(40%GF/GFRP)/clay	~40	~0.5	1000
	~20	0.5–1.0	
	~40	~0.5	1100
	~40	0.5–1.0	
(50%GF/GFRP)/clay	~60	~0.5	1000
	~60	0.5–1.0	
	~40	~0.5	1100
	~60	0.5–1.0	
(60%GF/GFRP)/clay	~20	~0.5	1000
	~20	0.5–1.0	
	~40	~0.5	1100
	~60	0.5–1.0	
	~40	1.0–1.4	

Figure 9 shows the specific strengths on bending of GFRP/clay and PA resin/clay ceramics. The *x*-axis expresses the resin mixing ratio. The specific strengths of GFRP/clay ceramics were relatively higher than that of the PA resin/clay ceramic without glass fiber. Particularly, although the specific strength of PA resin/clay ceramic significantly decreased with increasing resin mixing ratio when using the resin with a particle size of 0.5–1.0 mm, those of GFRP/clay ceramics did not decrease as much. Therefore, the GFRP/clay ceramics were reinforced by the glass fibers. The results indicate that ceramics with a light weight and high strength could be produced by mixing crushed GFRP with clay before firing. The mechanism by which glass fibers strengthen the ceramics is thought to be that the glass fibers bridged the circumference voids, which reinforced the material around the void [16].

Here, the specific strength of the ceramic with 60%GF/GFRP fired at 1,000 ℃ was lower than that of the ceramic with 40%GF/GFRP. The following can be considered as the cause:

(1) 60%GF/GFRP contained shorter glass fibers than 40%GF/GFRP.
(2) 60%GF/GFRP contained thinner glass fibers than 40%GF/GFRP.
(3) The ratio of glass fibers to clay was too large, which reduced sintering between glass fibers and clay.

Figure 10a shows the particle size distributions of the inorganic matter (glass fibers) in GFRPs, which were sifted with a 0.5-mm mesh screen. Figure 10b shows microscope images of the surface structures on the ceramics with 40%GF/GFRP and 60%GF/GFRP, which were made under the conditions that the particle size, mixing ratio of GFRP, and firing temperature were ~0.5 mm, 40%, and 1,000 ℃, respectively. Here, the inorganic matter was prepared by heating the GFRP powder after sifting at 400 ℃. The measurement of the particle size was performed on the basis of JIS Z-8825:2013 using a laser diffraction particle size analyzer (Sald-2100, Shimadzu Corp., Japan).

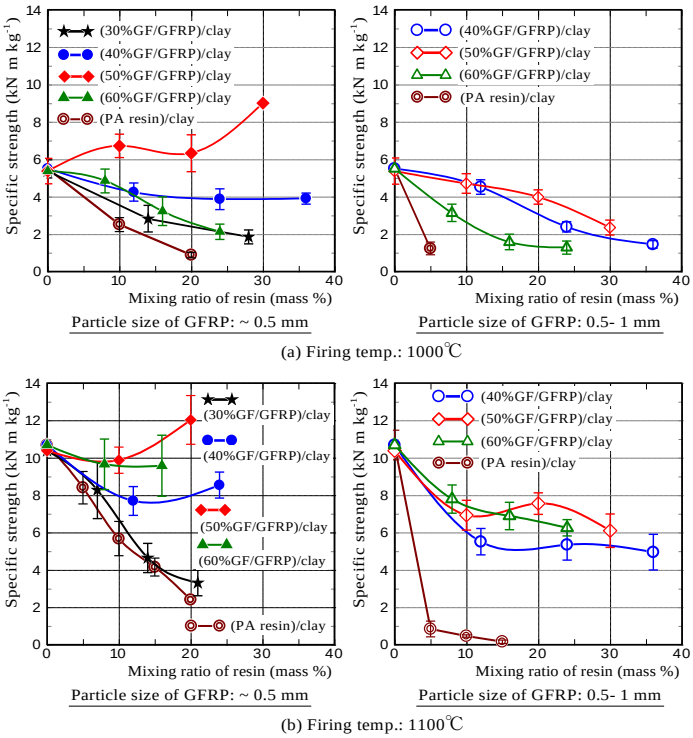

Figure 9. Bending strength versus porosity on GFRP/clay ceramics.

In Figure 10a, no significant difference in the size of inorganic matter in GFRPs is seen after sifting. However, in Figure 10b, it seems that particulates in the clay structure of the 60%GF/GFRP ceramic, which were formed by sintering of glass fibers, were smaller than those of the 40%GF/GFRP ceramic. This is thought to be because 60%GF/GFRP contained glass fibers thinner than those in 40%GF/GFRP. Therefore, we currently presume that the strength of the 60%GF/GFRP ceramic was lower than that of the 40%GF/GFRP ceramic. However, there may also be other factors requiring further investigation. The specific strength of the 60%GF/GFRP ceramic fired at 1,100 ℃ was higher than that of the 40%GF/GFRP ceramic presumably because the glass fibers and clay matrix were sintered more strongly than those in the 40%GF/GFRP ceramic due to the lower shrinkage start temperature of the glass fibers.

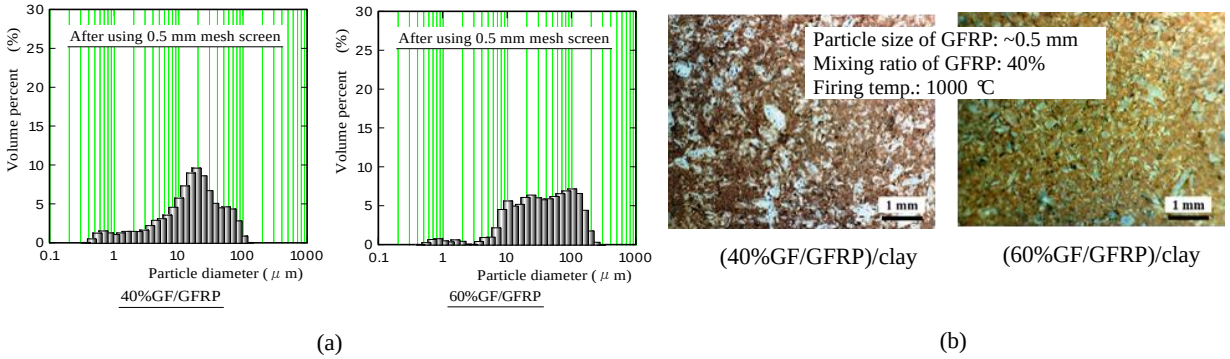

Figure 10. (a) Particle size distributions of inorganic matter in GFRP sifted using a 0.5-mm mesh screen, and examples of microscope images of the ceramic surface structures.

Figure 11 shows the bending strength versus porosity for GFRP/clay ceramics and PA resin/clay ceramic without glass fiber. It has been found that the GFRP/clay ceramic had a higher strength against the equivalent porosity than that of the ceramic without glass fiber. The results indicate that mixing GFRP with clay enabled us to produce ceramic with a high porosity, that is, a large pore size in the clay structure, because the clay structure was reinforced by glass fiber. This is the great advantage of using waste GFRP as a raw material to produce porous ceramics.

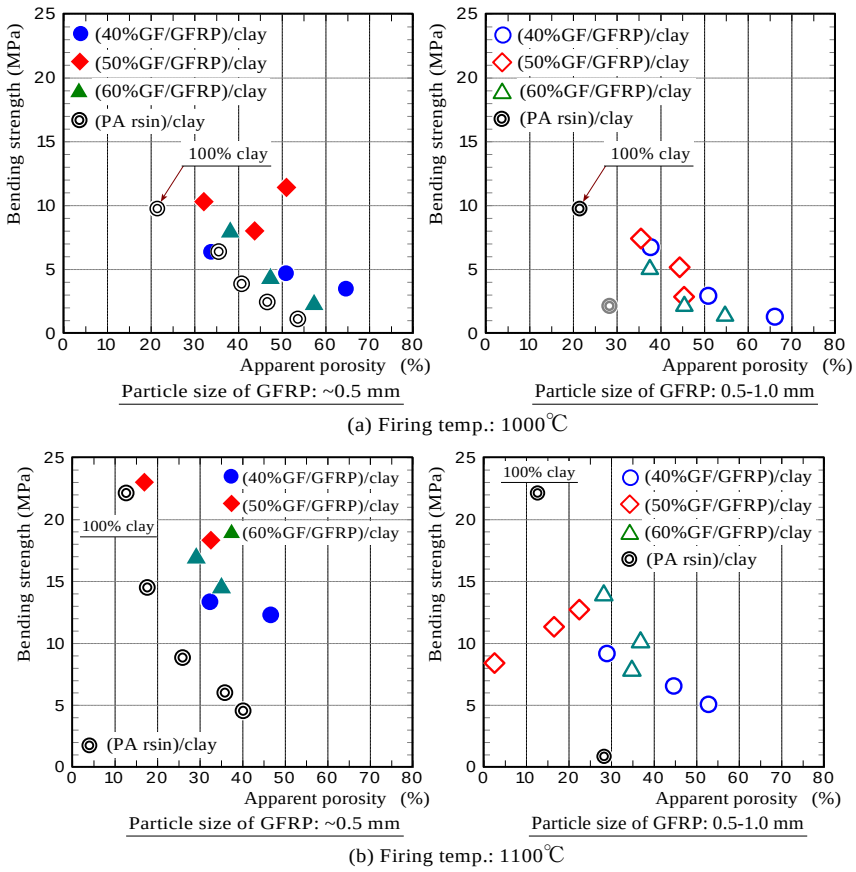

Figure 11. Bending strength versus porosity for GFRP/clay ceramics.

3.3. Ceramic compressive strength

Figure 12 shows the compressive strengths of GFRP/clay ceramics. The ceramic compressive strength decreased with increased GFRP mixing ratio for the same reason that the bending strength decreased. The compressive strength criterion for water-permeable paving blocks is 17 MPa or greater [23]. Table 3 shows manufacturing conditions of GFRP/clay ceramics that satisfy the compressive strength criterion. Although most ceramics fired at 1,000 ℃ did not meet this criterion due to the poor strength of the clay matrix, some GFRP/clay ceramics fired at 1,100 ℃ met this criterion.

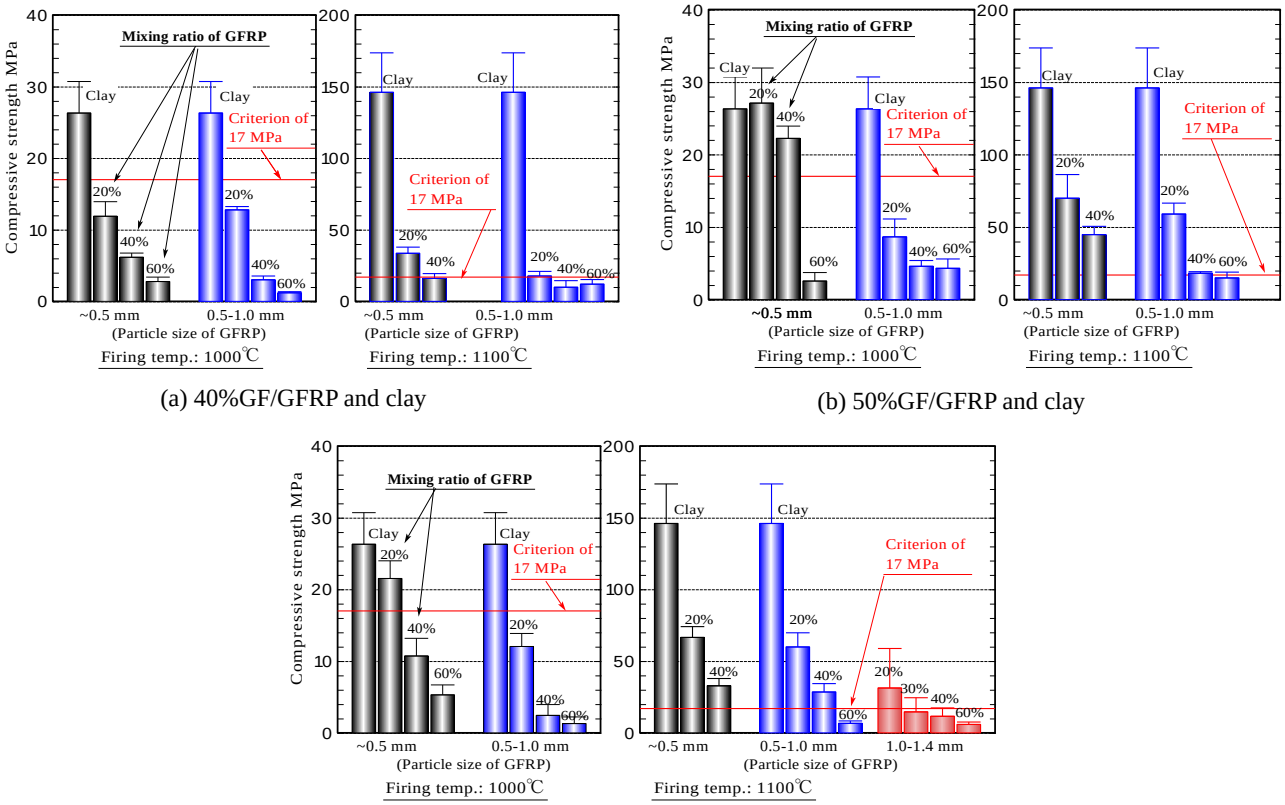

Figure 12. Compressive strength of GFRP/clay ceramics.

Table 3. Manufacturing conditions of GFRP/clay ceramics that satisfy the bending strength criterion of 17 MPa or greater.

Ceramic type	GFRP mixing ratio (mass%)	GFRP particle size (mm)	Firing temp (℃)
(40%GF/GFRP)/clay	~40	~0.5	1100
	~20	0.5–1.0	
(50%GF/GFRP)/clay	~40	~0.5	1000
	~40	~0.5	1100
	~40	0.5–1.0	
(60%GF/GFRP)/clay	~20	~0.5	1000
	~40	~0.5	1100
	~40	0.5–1.0	
	~20	1.0–1.4	

3.4. Ceramic water permeability

Figure 13 shows coefficients of water permeability of GFRP/clay ceramics and provides examples of SEM images of pores in the structures. Many GFRP/clay ceramics allowed water to pass through, although ceramics made from clay alone did not. The resin component in the GFRP is thought to have decomposed during the firing process, forming many interconnected pores in the

ceramic structure. Generally, the higher the mixing ratio of GFRP, the higher the ceramic permeability because the ceramic porosity increased.

A water permeability coefficient of 0.01 cm s^{-1} or greater is required for water-permeable paving blocks. A paving block with this coefficient allows a rainfall of 50 mm/h or greater to pass through [23]. Table 4 shows manufacturing conditions of GFRP/clay ceramics that satisfy the required criterion. It has been found that some of ceramics made by mixing GFRP with clay at mixing ratios of 40%–60% meet this criterion.

Figure 14 shows examples of the pore size distributions of the GFRP/clay ceramics. Ceramic made from clay alone had pore sizes of several micrometers or less. GFRP/clay ceramics had pore sizes from several to several hundreds of micrometers. Most ceramics with a permeability coefficient of 0.01 cm s^{-1} or greater possessed porosities higher than 30%, and mainly included pores measuring 100–300 μm in the ceramic structure.

Table 5 shows the manufacturing conditions for the ceramics that satisfy all the criteria required for water-permeable paving blocks. It is expected that water-permeable paving blocks can be produced by adjusting the mixing ratio of GFRP, its particle size, and firing temperature.

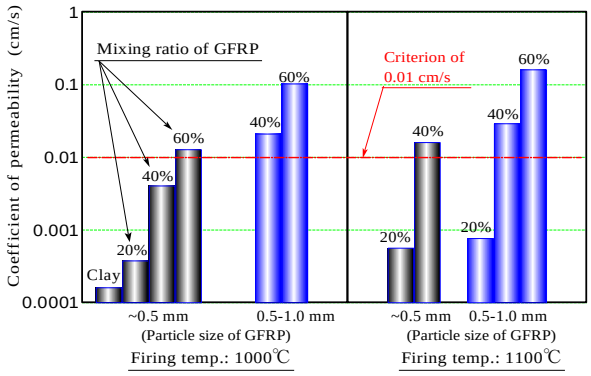

40%GF/GFRP and clay

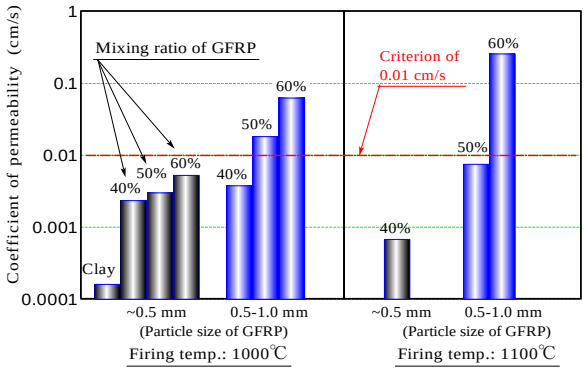

50%GF/GFRP and clay

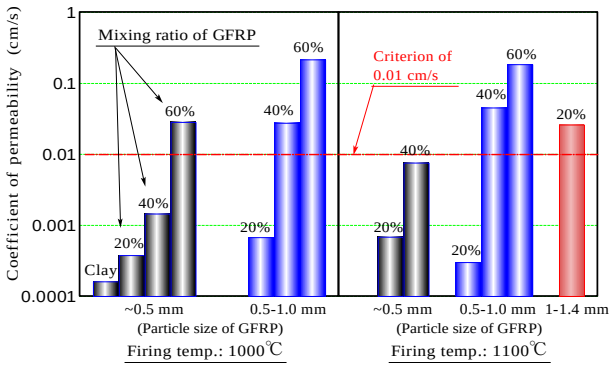

60%GF/GFRP and clay

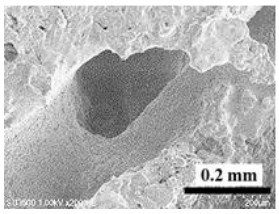

Particle size of GFRP: 0.5-1.0 mm
Mixing ratio of GFRP: 40%
Firing temp.: 1100 ℃

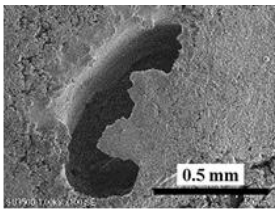

Particle size of GFRP: 1.0-1.4 mm
Mixing ratio of GFRP: 20%
Firing temp.: 1100 ℃

SEM images of 60%GF/GFRP and clay

Figure 13. Permeability of GFRP/clay ceramics and SEM images of pores in the structures.

Table 4. GFRP/clay ceramic manufacturing conditions necessary for creating ceramic with a coefficient of permeability of 0.01 cm s^{-1} or greater.

Ceramic type	GFRP mixing ratio (mass%)	GFRP particle size (mm)	Firing temp. (℃)
(40%GF/GFRP)/clay	60	~0.5	1000
	40–60	0.5–1.0	1000
	40–60	0.5–1.0	1100
(50%GF/GFRP)/clay	50–60	0.5–1.0	1000
	60	0.5–1.0	1100
(60%GF/GFRP)/clay	60	~0.5	1000
	40–60	0.5–1.0	1000
	40–60	0.5–1.0	1100
	20	1.0–1.4	1100

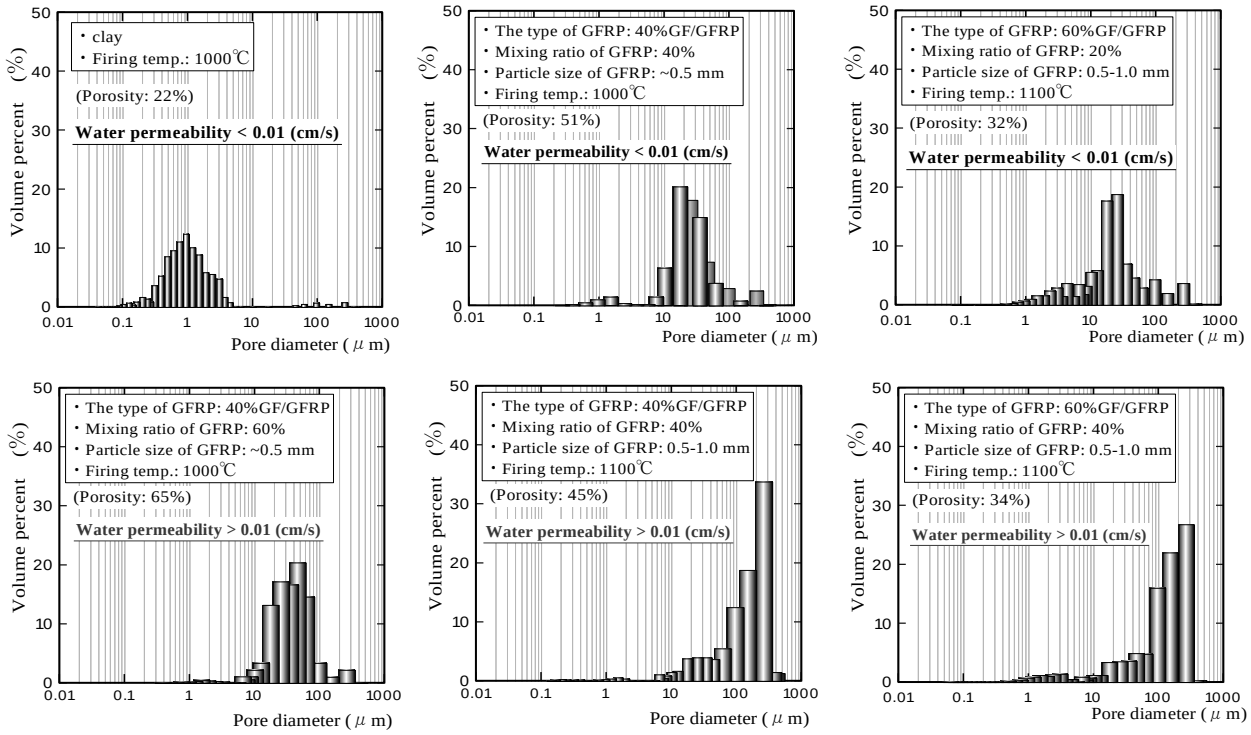

Figure 14. Pore size distributions.

Table 5. Manufacturing conditions of ceramics that satisfy all required criteria for paving blocks.

Ceramic type	GFRP mixing ratio (mass%)	GFRP particle size (mm)	Firing temp (℃)
(40%GF/GFRP)/clay	60	~0.5	1100
(60%GF/GFRP)/clay	40	0.5–1.0	1100
	20	1.0–1.4	1100

4. Conclusion

This study examined whether ceramics that satisfy both the strength and permeability criteria for water-permeable paving blocks could be produced by mixing crushed GFRP with clay and then firing the resultant mixture. Various specimens were made by adjusting the mixing ratio of clay and GFRP, the particle size of GFRP, and the firing temperature using three types of GFRPs, which contained glass fibers of approximately 40, 50, and 60 mass%. Bending strength, compressive strength, and permeability tests were then carried out on the samples. The results indicated that ceramics satisfying the criteria for water-permeable paving blocks could be produced under several specific manufacturing conditions. It is expected that GFRP/clay ceramics would be suitable for use in water-permeable paving blocks to counteract the effects of sudden heavy rain.

Finally, we will use byproducts such as sprues and runners, which are produced during the manufacture of plastic merchandise, as a raw material for GFRP/clay ceramics. It is relatively easy to collect the byproducts, which are discarded in large quantities as industrial waste. In addition, the type and grade of the waste GFRP is already known in most cases. It is considered to be an effective means to lower the manufacturing cost of GFRP/clay ceramics.

Acknowledgments

This work was funded by the Japan Society for the Promotion of Science, Kakenhi Grant 16K00614. We thank Bryan Schmidt from Edanz Group (www.edanzediting.com/ac) for editing a draft of this manuscript.

Conflict of interest

The authors declare no conflict of interest.

References

1. Ministry of the Environment Government of Japan ed. (2010) Annual Report on the Environment, the Sound Material-Cycle Society and the Biodiversity in Japan, Our Responsibility and Commitment to Preserve the Earth, Challenge 25: 1–169.
2. Plastic waste management institute ed. (2016) An Introduction to Plastic Recycling, 1–33.
3. Nagaoka T (2008) Value-Added Recycling of Disposal Plastics. *J JSTP* 49: 175–179.
4. Yang Y, Boom R, Irion B, et al. (2012) Recycling of Composite Materials. *Chem Eng Process* 51: 53–68.
5. Materials science society of Japan ed. (1999) *Global environment and materials*. Shokabo Co., Ltd., Tokyo, 61–74 (in Japanese).
6. WON JP, Jang CI, Lee SJ, et al. (2010) Long term performance of recycled PET fiber-reinforced cement composites. *Constr Build Mater* 24: 660–665.
7. Foti D, Paparella F (2014) Impact behavior of structural elements in concrete reinforced with PET fibers. *Mech Res Commun* 57: 57–66.
8. Akçaözoğlua S, Atişb CD, Akçaözoğluc K (2010) An investigation on the use of shredded waste PET bottle as aggregate in lightweight concrete. *Waste Manage* 30: 285–290.

9. Foti D (2013) Use of recycled waste pet bottles fibers for the reinforcement of concrete. *Compos Structu* 96: 396–404.
10. Mohammadi Y, Singh Sp, Kaushik SK (2008) Properties of steel fibrous concrete containing mixed fibres in fresh and hardened state. *Constr Build Mater* 22: 956–965.
11. Khaloo A, Raisi EM, Hosseini P, et al. (2014) Mechanical performance of self-compacting concrete reinforced with steel fibers. *Constr Build Mater* 51: 179–186.
12. Mazaheripour H, Ghanbarpour S, Mirmoradi SH, et al. (2011) The effect of polypropylene fibers on the properties of fresh and hardened lightweight self-compacting concrete. *Constr Build Mater* 25: 351–358.
13. Yesilata B, Isiker Y, Turgut P (2009) Thermal insulation enhancement in concretes by adding waste PET and rubber pieces. *Constr Build Mater* 23: 1878–1882.
14. Kinoshita H, Kaizu K, Takeda T, et al. (2010) Development of high strength porous specimen by Recycling of Waste Glass Fiber Reinforced Plastics. *T Jpn Soc Mech Eng* 76: 1507–1513.
15. Kinoshita H, Nakazono T, Oyamada M, Yet al. (2011) Development of high-strength porous tiles produced by recycling glass fibers in waste GFRP: Influence of particle size of GFRP on properties of tiles. *T Jpn Soc Mech Eng* 11: 241–248.
16. Kinoshita H, Kaizu K, Hasegawa S, et al. (2013) Production and Material Properties of Ceramic From Waste Glass Fiber Reinforced Plastic. *J Environ Eng* 8: 27–40.
17. Yasui K, Goto S, Kinoshita H, et al. (2016) Ceramic waste glass fiber-reinforced plastic-containing filtering materials for turbid water treatment. *Environ Earth Sci* 75: 1135.
18. Beeldens A, Herrier C (2007) Water-pervious pavement blocks environmentally compatible and cost-efficient water treatment at large road and parking areas. *Betonwerk Fertigteil-Technik* 73: 12–24.
19. Sriravindrarajah R, Mohammad KJ, Singh A (2013) Permeability and drying of pervious concrete pavers, *7th International Structural Engineering and Construction Conference*: New Developments in Structural Engineering and Construction, 1703–1707.
20. Drake JAP, Bradford A, Marsalek J (2013) Review of environmental performance of permeable pavement systems. *Water Qual Res J Can* 48: 203–222.
21. Tanaka M (1980) *Clay hand book*. Gihoudou Shuppan Co. Ltd. Tokyo, 408–445 (in Japanese).
22. Yasuda Y, Kinoshita H, Yasui K, et al. (2016) Ceramics utilizing glass fiber-reinforced plastic as civil engineering materials to counteract the heat island phenomenon. *Mech Eng J* 3: 16-00078.
23. Architectural Institute of Japan ed. (2009) *Japanese Architectural Standard Specification JASS 7 Masonry Work*. MARUZEN-YUSHODO Co., Ltd., Tokyo, 329–343.
24. Sakka S (1985) Dictionary of glass. Asakura Publishing Co., Ltd., Tokyo, 28 (in Japanese).
25. Central Glass Co. Ltd. home page, General characteristics of long glass fiber. Available from: http://www.centralfiberglass.com/jp/glass_fiber/outline/index.html.
26. Yamada M (1992) High Strength Phenolic Molding Compounds. *J Thermosetting Plast* 13: 44–58.